Theoretical investigations on phase stability, elastic constants and electronic structures of D022- and L12-Al3Ti under high pressure

ARTICLE *in* JOURNAL OF ALLOYS AND COMPOUNDS · NOVEMBER 2013

Impact Factor: 3 · DOI: 10.1016/j.jallcom.2012.12.135

(This is a sample cover image for this issue. The actual cover is not yet available at this time.)

Journal of Alloys and Compounds 556 (2013) 214–220

Contents lists available at SciVerse ScienceDirect

Journal of Alloys and Compounds

journal homepage: www.elsevier.com/locate/jalcom

Theoretical investigations on phase stability, elastic constants and electronic structures of $D0_{22}$- and $L1_2$-Al_3Ti under high pressure

Jian Li [a,b,*], Ming Zhang [c], Xian Luo [b]

[a] School of Materials Science and Engineering, Xi'an Shiyou University, Xi'an 710065, China
[b] School of Materials, Northwestern Polytechnical University, Xi'an 710072, China
[c] School of Petroleum Engineering, Xi'an Shiyou University, Xi'an 710065, China

ARTICLE INFO

Article history:
Received 26 October 2012
Received in revised form 22 December 2012
Accepted 24 December 2012
Available online 3 January 2013

Keywords:
First-principles
Titanium trialuminide (Al_3Ti)
Phase stability
Elastic constants
High pressure

ABSTRACT

Phase stability, elastic and thermodynamic properties, and electronic structure of titanium trialuminide (Al_3Ti) with Ll_2 and $D0_{22}$ structures under pressure up to 40 GPa have been investigated using first-principles calculations. The equilibrium structure and formation energy show that $L1_2$-Al_3Ti is stable when the pressure is higher enough, approximately above than 20–30 GPa. The elastic constants, anisotropy index and Debye temperature of both phases increase with the pressure going up, and $L1_2$-Al_3Ti has better ductility, smaller anisotropy and lower Debye temperature than $D0_{22}$-$A1_3Ti$. The pressure-induced Ti-3d delocalization can strengthen its orbital hybridization with Al(s,p), which leads to stronger atomic bonding, and subsequently makes the $L1_2$-Al_3Ti more stable under high pressure.

1. Introduction

Titanium trialuminide (Al_3Ti) has many attractive characteristics, such as low density (~3.3 g/cm^3), high melting temperature (~1623 K), good oxidation resistance, high hardness, and large elastic modulus [1,2]. Although this intermetallic has these promising characteristics, actually, bulky Al_3Ti is hardly used as structural material, which mainly caused by its poor ductility and toughness, and this is commonly ascribed to its insufficient slip systems in its tetragonal $D0_{22}$ structure (space group $I4/mmm$) [1,3–6]. Recently, many experimental and theoretical studies have been undertaken in attempts to fulfil the structure transition from tetragonal $D0_{22}$-Al_3Ti to cubic $L1_2$-Al_3Ti for the purpose of increasing its slip systems. According to the literatures, adding ternary elements, especially transition metals, such as Fe, [7–10] Mn, [1,9–11] Cr, [1,7,9,10,12,13] Co, [9,10] Ni, [8–10] Cu, [8,9] Zn, [14] Zr, [15] V, [7] and La [16], is suggested as a possible route to the structure transformation, and consequently improve the ductility of $A1_3Ti$-based alloys.

Although the phase stabilizing effect and the $L1_2$ structure transition by adding ternary element for Al_3Ti have been discussed extensively, in further consideration, the effect of high pressure on the phase stability should be discussed, and the influence of phase stability under high pressure can be investigated by performing first-principles calculations [17–20]. However, according to our knowledge, there is scarcely report about the pressure-induced structural transition for Al_3Ti up to now. In this paper, an investigation on phase stability, elastic properties and atomic bonding of Al_3Ti under high pressure was performed using first-principles calculations. The formation energy, elastic constants and electronic structure of $D0_{22}$- and $L1_2$-Al_3Ti under the pressure range of 0–40 GPa were calculated.

2. Computational methodology

The first-principles calculations presented in this paper were accomplished using the CASTEP code (Cambridge Sequential Total Energy Package) [21,22], which was based on density functional theory (DFT), a plane-wave basis set was employed for the electronic wave-function expansion [23,24]. The core–valence interactions were described as ultra-soft pseudo-potentials (USPPs) [25]. The exchange correlation energy was treated with three different functionals: generalized gradient approximation (GGA) functionals of PBE [26] and PW91 [27,28], and local density approximation (LDA) CAPZ functional of Ceperley and Perdew et al. [29,30]. The valence electron configurations of Al $3s^23p^1$ and Ti $3s^23p^63d^24s^2$ are considered. The k points were set as $25 \times 25 \times 25$ and $40 \times 40 \times 22$ for bulk fcc-Al and hcp-Ti, and $20 \times 20 \times 20$ and $20 \times 20 \times 10$ for bulk $A1_3Ti$ with $L1_2$ and $D0_{22}$ structures respectively, which makes the separation of the reciprocal space around 0.01 Å^{-1}, the cut-off energy on the plane wave basis was set as 350 eV, and the self-consistent field (SCF) tolerance was set as 5×10^{-7} eV/atom. The convergence tests have been tested, and the above parameters are also accordance with the previous studies [31–33]. The crystal supercell geometries were fully optimized, and their ground states were obtained, in which the Broyden–Fletcher–Goldfarb–Shanno

* Corresponding author at: School of Materials Science and Engineering, Xi'an Shiyou University, Xi'an 710065, China. Tel.: +86 29 88382598.
E-mail address: lijian@xsyu.edu.cn (J. Li).

0925-8388/$ - see front matter © 2012 Elsevier B.V. All rights reserved.
http://dx.doi.org/10.1016/j.jallcom.2012.12.135

Table 1
Crystallographic data, lattice constants of bulk Al, Ti and Al_3Ti.

Phase	Space group (#)	Pearson symbol	Strukturbericht designation	Lattice constants (Å)	
				Present Calc.	Expt.
fcc-Al	*Fm*-3*m*(225)	*cF*4	A1	a = 4.0484[a] a = 4.0510[b] a = 3.9674[c]	a = 4.049 [46]
hcp-Ti	$P6_3/mmc$(194)	*hP*2	A3	a = 2.9422, c = 4.6563[a] a = 2.9374, c = 4.6464[b] a = 2.8672, c = 4.5397[c]	a = 2.944, c = 4.669 [46]
Tetragonal Al_3Ti	*I*4/*mmm*(139)	*tI*8	$D0_{22}$	a = 3.8507, c = 8.6332[a] a = 3.8497, c = 8.6325[b] a = 3.7678, c = 8.4618[c]	a = 3.8537, c = 8.5839 [47]
Cubic Al_3Ti	*Pm*-3*m*(221)	*cP*4	$L1_2$	a = 3.9854[a] a = 3.9842[b] a = 3.8997[c]	a = 3.967–4.05 [35]

[a] The calculations with GGA-PBE exchange correlation functional in this work.
[b] The calculations with GGA-PW91 exchange correlation functional in this work.
[c] The calculations with LDA-CAPZ exchange correlation functional in this work.

minimization scheme [34] was used to minimize the total energy and interatomic force on each atom to the convergence level of 5×10^{-6} eV/atom and 0.01 eV/Å, respectively.

In the present study, the crystal structures of Al_3Ti were built based on the data of previous experiments and calculations [31,35,36]. After fully optimizations, the calculated equilibrium lattice constants and previous experimental data are listed in Table 1, the elastic constants and formation energy $\Delta E_f(Al_3Ti)$ are listed in Table 2. The lattice constants calculated with LDA-CAPZ potential is rather smaller than the results of GGA-PBE and GGA-PW91, which indicates the "over-binding effect" reported in other LDA calculations [37–41]. The equilibrium lattice constants calculated with GGA-PBE functional are most close to the previous experimental data in Table 1. In Table 2, the GGA-PBE results of elastic constants have better agreements with previous theoretical results [42–44] and experimental data [45] than the results calculated with GGA-PW91 and LDA-CAPZ functionals. For the $D0_{22}$ structure, by comparing GGA-PBE calculated elastic constants with experimental data [45], it shows very good agreement (less than 5.2%) for the values of C_{13}, C_{33} and C_{44}. However, the deviation of C_{11}, C_{12} and C_{66} comparing with the experimental data are slightly larger, the errors are about 12.5%, 43.9% and 8.0%, respectively. Furthermore, it is worthy to note that the same tendency exists in the previous calculations [42–44].

3. Results and discussion

3.1. Phase stability and formation energy

The formation energy $\Delta E_f(Al_3Ti)$ per atom is defined by the following equation [52]:

$$\Delta E_f(Al_3Ti) = \frac{1}{4}[E_{total}(Al_3Ti) - 3E_{bulk}(Al) - E_{bulk}(Ti)], \quad (1)$$

where $E_{total}(Al_3Ti)$ is the total energy per formula of equilibrium Al_3Ti structure; $E_{bulk}(Al)$, and $E_{bulk}(Ti)$ are the total energy per atom of fully relaxed fcc-Al and hcp-Ti, respectively. After the structures fully optimized, the formation energy of both phases under zero temperature and various pressure ranging from 0 to 40 GPa have been calculated, the results are summarized in Table 3. The results calculated with GGA-PBE and PW91 are very similar (the max numerical error of formation energy is only 3% for Ll_2-$A1_3Ti$ under 5 GPa), and their results agree well with previous calculations [35,43,48,49], however, the LDA results differs vastly with the GGA results (the max numerical error of formation energy is 60% for $D0_{22}$-$A1_3Ti$ under 5 GPa). That suggests the numerical errors of formation energy strongly depends on the exchange-correlation functional [53]. And from Table 2, one can further find that the formation energies under 0 GPa calculated with GGA-PBE and GGA-PW91 are more close to the experimental data [50] (the deviations are about 2%), and LDA-CAPZ calculated result has the largest deviation of more than 4%. The large errors of LDA formation energy calculations are due to the overestimation of local density approximation method [51].

Table 2
Elastic constants and formation energy $\Delta E_f(Al_3Ti)$ of $L1_2$- and $D0_{22}$-Al_3Ti.

Phase	Elastic properties (GPa)							$\Delta E_f(Al_3Ti)$ (kJ/mol)[a]
	C_{11}	C_{12}	C_{13}	C_{33}	C_{44}	C_{66}	B_0	
$D0_{22}$-Al_3Ti	190.39	83.05	43.14	214.68	92.24	125.85	103.69	−38.280[b]
	190.49	81.44	42.47	211.09	90.60	123.35	102.61	−38.378[c]
	210.85	92.43	46.28	240.61	104.74	143.73	114.60	−40.816[d]
	192.3	82.7	44.9	212.5	93.0	128.4	103.3	−38.895 [43][e]
	194.5	87.9	47.6	219.8	93.8	129.5	108.3 [42][e]	−39.30 [35][e]
	192	84	49	216	94	122	107 [44][e]	−39.505 [48][e]
	–	–	–	–	–	–	–	−38.11 [49][e]
	217.7	57.7	45.5	217.5	92.0	116.5	105.6 [45][f]	−39.2 [50][f]
$L1_2$-Al_3Ti	184.40	64.21	–	–	74.61	–	104.27	−35.499[b]
	184.32	62.41	–	–	72.89	–	103.05	−35.741[c]
	207.54	69.05	–	–	87.29	–	115.21	−38.609[d]
	183.9	62.6	–	–	73.5	–	103.6	−36.583 [43][e]
	190.2	67.5	–	–	77.0	–	108.4 [42][e]	−35.651 [51] [e]
	192	65	–	–	74	–	107 [44][e]	−36.614 [48][e]
	–	–	–	–	–	–	–	−35.35 [49][e]

[a] For the calculation of formation energy, the reference states are fcc-Al and hcp-Ti under 0 K and 0 GPa.
[b] Calculations with GGA-PBE functional in this work under 0 K and 0 GPa.
[c] Calculations with GGA-PW91 functional in this work under 0 K and 0 GPa.
[d] Calculations with LDA-CAPZ functional in this work under 0 K and 0 GPa.
[e] Other first-principle calculation results at zero temperature.
[f] Experimental results at ambient temperature and pressure.

Table 3
The total energy E_{total}, formation energy ΔE_f, lattice constants and equilibrium volume V_0 of $L1_2$- and $D0_{22}$-Al_3Ti under various pressures and temperature $T = 0$ K[a].

Pressure (GPa)	0	5	10	15	20	25	30	35	40
$D0_{22}$-Al_3Ti									
a (Å)	3.8507	3.7959	3.7495	3.7092	3.6733	3.641	3.6116	3.5846	3.5596[b]
	3.8497	3.7948	3.7482	3.7079	3.6720	3.6396	3.6102	3.5831	3.5579[c]
	3.7678	3.7192	3.6770	3.6401	3.6069	3.5769	3.5494	3.5240	3.5005[d]
c (Å)	8.6332	8.5012	8.3908	8.2953	8.2120	8.1376	8.0695	8.0077	7.9504[b]
	8.6325	8.4978	8.3867	8.2906	8.2071	8.1322	8.0642	8.0026	7.9458[c]
	8.4618	8.3437	8.2438	8.1563	8.0786	8.0087	7.9454	7.8870	7.8330[d]
c/a	2.242	2.240	2.238	2.236	2.236	2.235	2.234	2.234	2.234[b]
	2.242	2.239	2.238	2.236	2.235	2.234	2.234	2.233	2.233[c]
	2.246	2.243	2.242	2.241	2.240	2.239	2.239	2.238	2.238[d]
V_0 (Å^3/atom)	16.002	15.311	14.746	14.266	13.851	13.485	13.157	12.862	12.592[b]
	15.992	15.297	14.728	14.248	13.832	13.466	13.138	12.843	12.573[c]
	15.016	14.426	13.932	13.509	13.138	12.808	12.512	12.244	11.997[d]
ΔE_f (kJ/mol)	−38.280	8.800	54.000	97.636	139.932	181.068	221.151	260.300	298.600[b]
	−38.377	8.659	53.811	97.392	139.630	180.699	220.723	259.812	298.053[c]
	−40.816	3.456	44.910	86.184	126.269	165.304	203.399	240.650	277.126[d]
$L1_2$-Al_3Ti									
a (Å)	3.9854	3.9281	3.8792	3.8368	3.7992	3.7653	3.7345	3.7062	3.6801[b]
	3.9842	3.9264	3.8773	3.8350	3.7972	3.7634	3.7326	3.7043	3.6782[c]
	3.8997	3.8480	3.8038	3.7649	3.7301	3.6986	3.6698	3.6433	3.6186[d]
V_0 (Å^3/atom)	15.825	15.153	14.594	14.120	13.709	13.346	13.021	12.727	12.460[b]
	15.812	15.132	14.573	14.100	13.688	13.325	13.001	12.708	12.441[c]
	14.826	14.245	13.759	13.341	12.974	12.648	12.356	12.090	11.846[d]
ΔE_f (kJ/mol)	−35.499	11.016	55.746	98.932	140.792	181.492	221.161	259.902	297.801[b]
	−35.741	10.694	55.358	98.481	140.276	180.914	220.518	259.198	297.039[c]
	−38.609	5.100	46.025	86.782	126.367	164.913	202.531	239.310	275.326[d]

[a] For the calculation of formation energy, the reference states are fcc-Al and hcp-Ti under the pressure and zero temperature.
[b] Calculations with GGA-PBE functional in this work.
[c] Calculations with GGA-PW91 functional in this work.
[d] Calculations with LDA-CAPZ functional in this work.

Although the exchange correlation functionals have an influence on the formation energy calculation, some valuable points can still be deduced. First, the formation energy will increase, while the lattice constants and volume will decrease along with the pressure increasing. Second, the formation energies of $D0_{22}$-$A1_3Ti$ are smaller than the ones of Ll_2-$A1_3Ti$ when the pressure is below 20 GPa, while the opposite situation exists when the pressure is above 30 GPa. In the range of 20–30 GPa, the difference between the formation energies of both structures depends on the exchange correlation functionals. Which suggests the Ll_2-$A1_3Ti$ will be more stable when the pressure is higher enough, approximately above than 20–30 GPa.

Actually, the Gibbs free energy should be used to compare the phase stability between the both structures, because all calculations in our work are performed under the temperature $T = 0$ K, so the relative stability of different structures can be deduced from the pressure dependence on enthalpy [54,55]. The enthalpy difference per formula $H(L1_2)$-$H(D0_{22})$ under various pressure are calculated and shown in Fig. 1. The pressure corresponding to $H(L1_2)$-$H(D0_{22})$ approaching zero is the transition pressure, it shows that the $D0_{22}$-Al_3Ti will transform to the $L1_2$ structure when the pressure is over ~30 GPa, ~28 GPa, ~21 GPa calculated with functionals of GGA-PBE, GGA-PW91, LDA-CAPZ, respectively. It is consistent with the above conclusion deduced from the formation energies under various pressures. And there are volume drop per atom of $\Delta V/V = 1.0$–1.2% with the three different functionals as shown in Fig. 2.

3.2. Elastic constants and thermodynamic properties

The elastic constants of solids have a direct relation to their mechanical and thermodynamic properties. Commonly, the single crystal's elastic constants C_{ij} can be obtained by calculating the total energy as a function of appropriate strains [42–44]. To calculate the elastic constants, a serial of deformed cells (strain) are introduced and optimized to calculate the tensor of elastic constants. The elastic strain energy U of a deformed crystal cell is given as [56]:

$$U = \frac{\Delta E}{V_0} = \frac{1}{2}\sum_{ij} C_{ij} e_i e_j \quad (2)$$

where ΔE is the energy difference of deformed cell relative to the unstrained cell, V_0 is the volume of the equilibrium cell without any deformation, C_{ij}s are the elastic constants, e_i and e_j are strain.

For the $L1_2$ structure, there are three independent elastic constants: $C_{11} = C_{22} = C_{33}$, $C_{12} = C_{13} = C_{23}$, $C_{44} = C_{55} = C_{66}$; for the $D0_{22}$ structure, there are six independent constants: $C_{11} = C_{22}$, C_{12}, $C_{13} = C_{23}$, C_{33}, $C_{44} = C_{55}$, C_{66}. The obtained monocystal quantities,

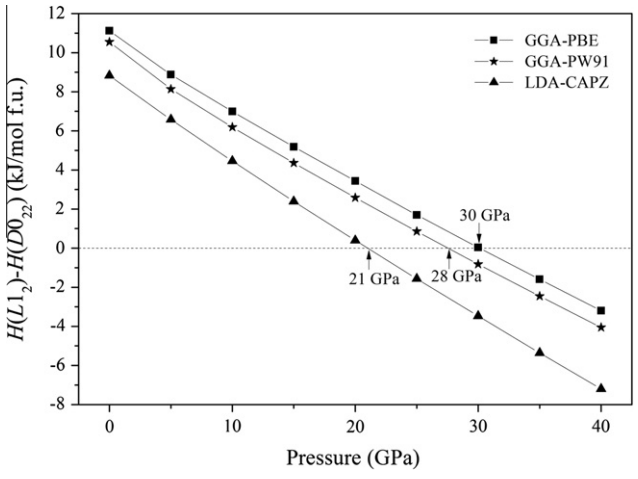

Fig. 1. Calculated enthalpy difference of $L1_2$-Al_3Ti relative to the $D0_{22}$ structure as a function of pressure, the structural transition point induced by pressure are marked by arrows.

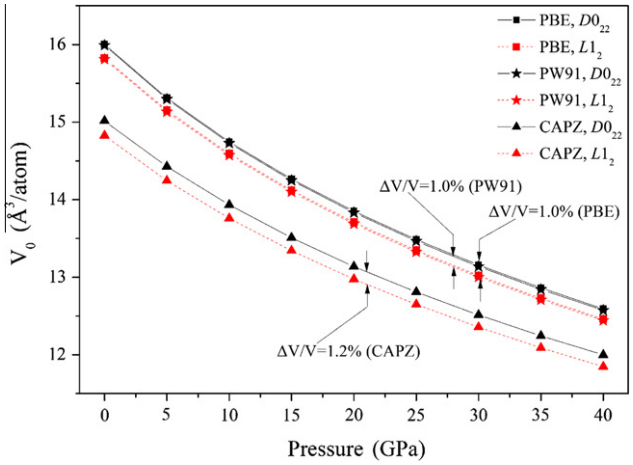

Fig. 2. Calculated volume–pressure relationship for $D0_{22}$- and $L1_2$-Al_3Ti with different exchange correlation functionals.

such as these elastic constants, cannot accurately stand for the properties of polycrystalline materials, so they should be further calculated and rectified. The polycrystalline mechanical quantities, such as bulk modulus (B), shear modulus (G), Young's modulus (E), Poisson's ratio (v), can be calculated from these independent elastic constants.

There are three different algorithms corresponding to different bound to calculate these polycrystalline mechanical quantities: the Voigt bound is obtained by the average polycrystalline modules based on an assumption of uniform strain throughout a polycrystal, and it is the upper limit of the actual effective modules; while the Reuss bound is obtained by assuming a uniform stress, and it is the lower limit of the actual effective modules; the arithmetic average of Voigt and Reuss bounds is termed as the Voigt–Reuss–Hill approximation. The formula for calculating these mechanical quantities can be given as follows: (1) for the cubic $L1_2$ structures, $B_V = B_R = (C_{11} + 2C_{12})/3$, $G_V = (C_{11} - C_{12} + 3C_{44})/5$, $G_R = 5(C_{11} - C_{12})C_{44}/[4C_{44} + 3(C_{11} - C_{12})]$ [57], (2) for the tetragonal $D0_{22}$ structures, $B_V = (1/9)[2(C_{11} + C_{12}) + C_{33} + 4C_{13}]$, $B_R = C^2/M$, $G_V = (1/30)(M + 3C_{11} - 3C_{12} + $ ce:hsp sp="0.25"/>$12C_{44} + 6C_{66})$, $G_R = 15\{(18B_V/C^2) + [6/(C_{11} - C_{12})] + (6/C_{44}) + (3/C_{66})\}^{-1}$; $M = C_{11} + C_{12} + 2C_{33} - 4C_{13}$, $C^2 = (C_{11} + C_{12})C_{33} - 2(C_{13})^2$ [58], and (3) for the Voigt–Reuss–Hill approximation, $B_H = (1/2)(B_V + B_R)$, $G_H = (1/2)(G_V + G_R)$, the sub letter of V, R and H denote Voigt, Reuss bound and Hill approximation, respectively. The B_H and G_H are adopted in this paper to calculate Young's modulus E and Poisson's ratio v by the following formulas: $E = 9BG/(3B + G)$, $v = (3B - 2G)/[2(3B + G)]$ [59].

The elastic constants of $L1_2$- and $D0_{22}$-Al_3Ti under 0 GPa are calculated with GGA-PBE, GGA-PW91 and LDA-CAPZ functionals, the results and other experimental and computational data are presented in Table 2. As aforementioned, there are slightly large deviations between the experimental data [45] and our GGA-PBE calculated values of C_{11}, C_{12} and C_{66} for $D0_{22}$-Al_3Ti, however, comparing with other theoretical calculations [42,44], the agreements of GGA-PBE results are reasonable and acceptable. Besides that, Al_3Ti lattice constants and elastic constants under 0 GPa calculated with GGA-PBE are more closer to the experimental data (refers Table 1). As the further step, the elastic constants under high pressure in the range of 5–40 GPa are also calculated with GGA-PBE functional, and the results are listed in Table 4. The elastic constants and mechanical moduli increase with the pressure increasing, which indicates the materials will be stiffer and more difficult to be compressed with pressure increasing. The hardness and brittleness of the compounds also have a relation to the B/G value: according to Pugh's criterion [60], the compound with larger B/G ratio (>∼1.75) usually is ductile, and with smaller B/G ratio (<∼1.75) usually is brittle, thus, $L1_2$-Al_3Ti should exhibit better ductility than $D0_{22}$-Al_3Ti, and both structures will have larger ductility under high pressure than ambient pressure.

Elastic anisotropy index A^U for crystal with any symmetry was proposed by Ranganathan and Ostoja-Starzewski [61],

$$A^U = 5\frac{G_V}{G_R} + \frac{B_V}{B_R} - 6 \geqslant 0 \tag{3}$$

Zero value of A^U denotes isotropic single crystals, and the deviation from zero defines the extent of this crystal's anisotropy. For cubic symmetry, the relationship between the commonly used Zener anisotropy ratio A and A^U can be defined as $A^U = (6/5)(\sqrt{A} - 1/\sqrt{A})^2$. The results of $L1_2$- and $D0_{22}$-Al_3Ti calculated as per the equation are listed in Table 4. It shows $L1_2$-Al_3Ti has more isotropic features than $D0_{22}$-Al_3Ti, and the both structures' isotropy decrease with the pressure increasing.

Debye temperature (Θ_D) is a fundamental parameter for the materials' thermodynamic properties, and it is correlated with many physical properties such as specific heat, elastic constants and melting temperature. The experimental value of a solid usually can be calculated from the sound velocity [62]. In this paper, Debye temperatures of $L1_2$- and $D0_{22}$-Al_3Ti under ambient and high pressure are estimated with the elastic constant data. Θ_D may be estimated from the averaged sound velocity by the following equation [62]:

$$\Theta_D = \frac{h}{k}\left[\frac{3n}{4\pi}\left(\frac{N_A\rho_0}{M}\right)\right]^{\frac{1}{3}}\upsilon_m \tag{4}$$

where h is the Planck's constant, k is Boltzmann's constant, N_A is the Avogadro constant, n is the atoms number per molecule, M is the molecular weight, and ρ_0 is the density, respectively. The average sound velocity υ_m can be calculated as follows:

Table 4
Elastic constants C_{ij}, bulk modulus B, shear modulus G, Young's modulus E (all in GPa), Poisson's ratio and Elastic anisotropy index A^U of $L1_2$- and $D0_{22}$-Al_3Ti under various pressures.

Pressure (GPa)	$D0_{22}$-Al_3Ti					$L1_2$-Al_3Ti				
	0	10	20	30	40	0	10	20	30	40
$C11$	190.4	241.8	287.8	330.5	370.6	184.4	240.9	292.1	339.8	385.6
$C12$	83.1	119.7	154.4	188.1	220.7	64.2	93.3	120.5	146.5	171.9
$C13$	43.1	69.2	94.2	118.4	142.3	–	–	–	–	–
$C33$	214.7	279.4	342.1	391.8	442.6	–	–	–	–	–
$C44$	92.2	118.8	142.3	163.6	183.4	74.6	102	126.8	149.4	170.6
$C66$	125.8	161.8	193.8	223.3	250.6	–	–	–	–	–
B	103.7	142.1	178.1	211.4	243.8	104.3	142.5	177.7	210.9	243.1
G	87.2	108.1	126.2	141.8	156.1	68.4	89.6	108.4	125.5	141.4
E	204.3	258.6	306.3	347.6	385.9	168.4	222.2	270.3	314.1	355.4
v	0.17	0.2	0.21	0.23	0.24	0.23	0.24	0.25	0.25	0.26
B/G	1.19	1.31	1.41	1.49	1.56	1.52	1.59	1.64	1.68	1.72
A^U	0.39	0.53	0.66	0.77	0.88	0.06	0.13	0.19	0.23	0.27

Table 5
Debye temperature Θ_D of $L1_2$- and $D0_{22}$-Al_3Ti under various pressures.

Pressure (GPa)	0	10	20	30	40
Θ_D of $D0_{22}$-Al_3Ti (K)	664.2	731.4	783.6	824.5	859.9[a]
	558.29	649.36	716.25[b]	–	–
Θ_D of $L1_2$-Al_3Ti (K)	591.0	668.0	727.7	776.7	819.0[a]

[a] Calculations with GGA-PBE elastic constants of this work.
[b] Previous calculation of Ref. [49].

$$\upsilon_m = \left[\frac{1}{3}\left(\frac{2}{\upsilon_s^3}+\frac{1}{\upsilon_l^3}\right)\right]^{-1/3}, \text{ and } \upsilon_l = \left(\frac{3B+4G}{3\rho_0}\right)^{1/2}, \upsilon_s = \left(\frac{G}{\rho_0}\right)^{1/2} \quad (5)$$

where υ_l and υ_s are the longitudinal and shear sound velocities, respectively. The Debye temperatures of $L1_2$- and $D0_{22}$-Al_3Ti are calculated from the aforementioned values of the lattice parameters, the bulk modulus and shear modulus, and the results are listed in Table 5.

Nakamura and Kimura [45] calculated the Debye temperature of $D0_{22}$-Al_3Ti by measuring the velocity of ultrasonic waves at ambient pressure and temperature, and the value was 681 K. Because $L1_2$-Al_3Ti is metastable, its experimental Debye temperature can be hardly found in the literatures, Witczak et al. [63] measured the Θ_D of $L1_2$ Al_5CrTi_2 with ultrasonic pulse-echo method, their experimental value was 588 K. Our results of Θ_D at ambient pressure are in good accordance with these experimental literatures [45,63]. Boulechfar et al. [49] calculated the Θ_D of $D0_{22}$- and $L1_2$-$A1_3Ti$ under 0–20 GPa using first principles method, the results are listed in Table 5, and our results have acceptable agreements with their data.

In Debye theory, the Θ_D is the temperature of a crystal's highest normal mode of vibration, i.e., the highest temperature that can be achieved due to a single normal vibration. One can find that the Debye temperatures of both structures will increase with the pressure increasing, which indicates that the normal vibration of both crystals will enhance when the pressure increases. The $D0_{22}$-Al_3Ti has higher Θ_D than $L1_2$-Al_3Ti, and the gap of Θ_D between the both phases decrease with the pressure increasing.

3.3. Electronic structure and atomic bonding

For a deeper insight into the atomic bonding and electronic structure of $A1_3Ti$ under high temperature, the valence electron density distribution, density of states (DOS) and partial density of states (PDOS) are investigated with GGA-PBE functional. Fig. 3a–d illustrate the valence electron distribution of $L1_2$-$A1_3Ti$ and $D0_{22}$-$A1_3Ti$ along (1 1 0) plane under 0 GPa and 40 GPa, respectively. The PDOS of $L1_2$-Al_3Ti under 0 GPa and 40 GPa are presented in Fig. 4. The Γ point band composition of both phases under 0 GPa and 40 GPa are listed in Table 6.

The valence charge density distribution (Fig. 3) shows that both structures at 40 GPa have a strengthened valence electron interaction than at 0 GPa. The bonding charges of Ll_2-$A1_3Ti$ mainly locate at tetrahedral interstices along ⟨1 1 1⟩ directions, it is because the nearest-neighbor atoms of Ti-site leads to Ti-d hybridization around its local field [49,51,64]. And bonding charges of $D0_{22}$-Al_3Ti mainly locate along its ⟨1 1 2⟩ directions caused by the d orbital hybridization [49,51,64].

The PDOS plots of Ll_2-$A1_3Ti$ (Fig. 4) indicate that the left part of total DOS (below Fermi lever) is mainly contributed from Al atom, namely Al-3s and Al-3p, while the right part mainly comes from Ti atom, especially Ti-3d. Furthermore, the resonant peaks of PDOS plots can also confirm that the bonds of $L1_2$-Al_3Ti are mainly contributed from the electron orbitals hybridization of Ti-3d and Al(s,p) states [49,51,64]. By comparing DOS plots of $L1_2$-$A1_3Ti$ under 0 GPa and 40 GPa, one can easily find that the energy range of DOS under 40 GPa is widened, and has a shallower "valley" around Fermi level than the one under 0 GPa. Simultaneously, the PDOS of Al under 40 GPa shifts towards lower energy, while the PDOS of Ti under 40 GPa shifts towards higher energy, and the peak of Ti-3d around 2 eV under 40 GPa is lower than the one under 0 GPa. Considering the widened energy range, shallower "valley" and lower peak denote more non-localized features, and the wider bandwidth, especially the wider conduction band, denotes more "free electrons", one can know that the structure under 40 GPa has more metallic features than it at 0 GPa, thus, a better electrical conductivity of $L1_2$-Al_3Ti under high pressure will be anticipated.

Further, according to the Ti PDOS under 40 GPa shifts towards higher energy, and it has a lower peak than the one under 0 GPa, it is reasonable to conclude that pressure-induced delocalization of Ti electrons, especially Ti-3d, which strengthens the electron hybridization and atomic bonding between Ti and Al atoms. And subsequently, it improves the phase stability of $L1_2$-Al_3Ti, even though the phase exhibits more metallic features with the pressure increasing.

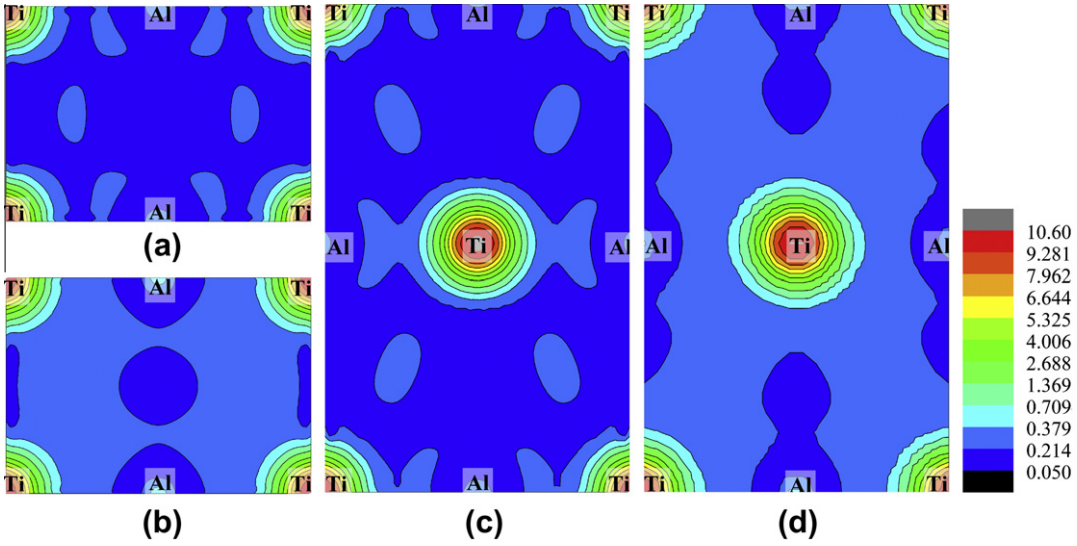

Fig. 3. Valence charge density (e/Å^3) distribution of $L1_2$- and $D0_{22}$-Al_3Ti under 0 GPa and 40 GPa along (1 1 0) plane: (a) $L1_2$, 0 GPa; (b) $L1_2$, 40 GPa; (c) $D0_{22}$, 0 GPa, (d) $D0_{22}$, 40 GPa.

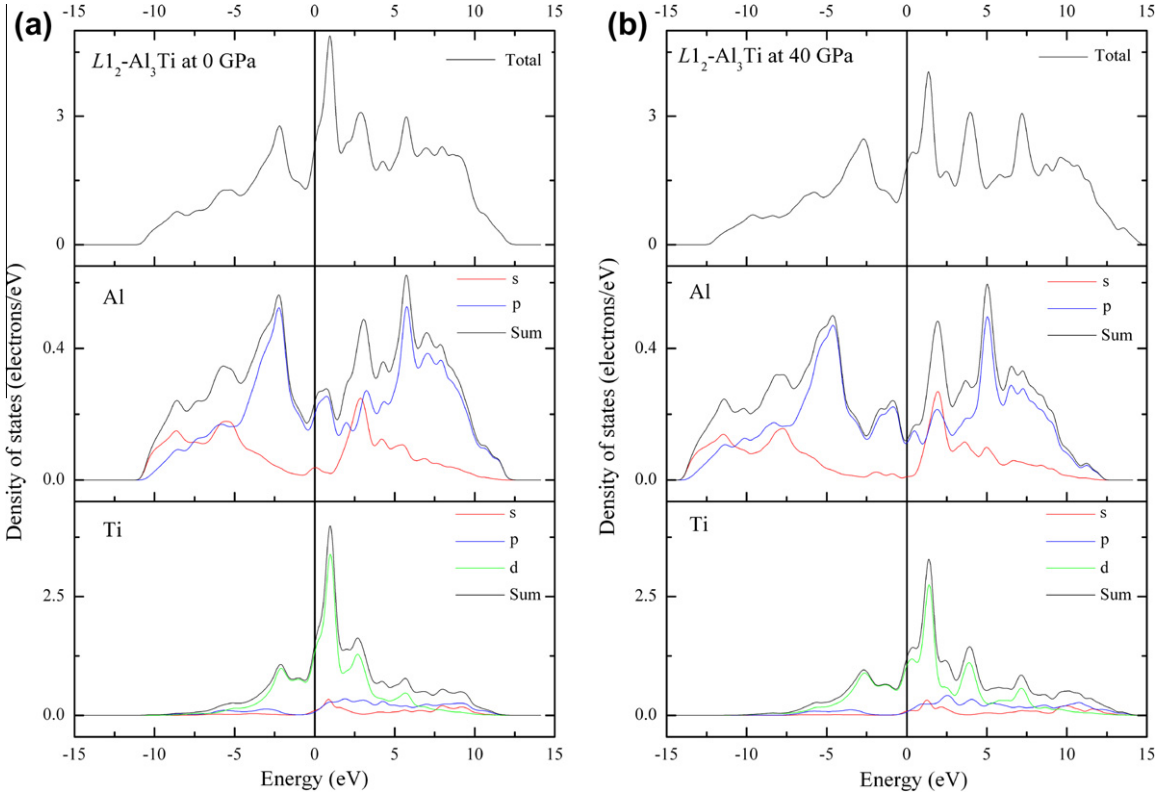

Fig. 4. Density of states (DOS) of $L1_2$-Al_3Ti under (a) 0 GPa and (b) 40 GPa.

From Table 6, the compositions for the lowest Γ point state of both structures are dominated by Al-s, and for $D0_{22}$-$A1_3Ti$, it is specifically the s component of Al2. From the second to fourth lowest Γ point states of both structures, and the fifth Γ point states of $D0_{22}$-$A1_3Ti$, they are dominated by the hybridization of Al-p and Ti-d. and the sixth Γ point states (the first unoccupied state) of $D0_{22}$-$A1_3Ti$ is mainly composed by Ti-d. The above features are consistent with the previous calculation [51]. More important is that, except for the fourth lowest state of both structures, all Ti-d components at Γ point under 40 GPa increase comparing with 0 GPa, which indicates the quantity and the hybridization of Ti-3d will be improved and strengthened under high pressure, and the stronger atomic bonding can be anticipated.

Table 6
Band composition at Γ point for $D0_{22}$- and $L1_2$-Al_3Ti under 0 GPa and 40 GPa.

Band number	Energy (eV)	Al1	Al2	Ti
$D0_{22}$-Al_3Ti at 0 GPa				
1	−10.00	*s* 26.67%; *p* 2.42%	*s* 57.92%; *p* 5.39%	*s* 6.45%; *p* 1.11%; *d* 0.03%
2	−2.86	*s* 5.54%; *p* 20.53%	*s* 12.38%; *p* 35.67%	*s* 3.04%; *p* 8.08%; *d* 14.75%
3	−2.60	*s* 5.81%; *p* 19.07%	*s* 12.06%; *p* 34.79%	*s* 2.69%; *p* 8.47%; *d* 17.11%
4	−1.37	*s* 2.77%; *p* 13.64%	*s* 3.51%; *p* 37.41%	*s* 1.34%; *p* 7.01%; *d* 34.32%
5	−0.93	*s* 2.13%; *p* 11.30%	*s* 1.94%; *p* 35.79%	*s* 0.95%; *p* 5.40%; *d* 42.49%
6	0.70	*s* 0.36%; p 6.79%	*s* 0.38%; p 10.47%	*s* 0.93%; *p* 1.90%; *d* 79.17%
$D0_{22}$-Al_3Ti at 40 GPa				
1	−11.27	*s* 29.36%; *p* 2.31%	*s* 62.49%; *p* 5.53%	*s* 0.21%; *p* 0.05%; *d* 0.04%
2	−3.08	*s* 3.56%; *p* 21.37%	*s* 11.81%; *p* 34.75%	*s* 2.65%; *p* 6.66%; *d* 19.20%
3	−2.87	*s* 4.81%; *p* 18.08%	*s* 11.88%; *p* 34.31%	*s* 2.25%; *p* 8.19%; *d* 20.48%
4	−1.91	*s* 3.11%; *p* 13.37%	*s* 5.14%; *p* 37.86%	*s* 1.64%; *p* 9.83%; *d* 29.05%
5	−0.81	*s* 2.10%; *p* 9.43%	*s* 1.26%; *p* 34.32%	*s* 1.11%; *p* 5.64%; *d* 46.14%
6	0.79	*s* 0.22%; *p* 6.11%	*s* 0.05%; *p* 11.17%	*s* 0.37%; *p* 2.24%; *d* 79.84%

Band number	Energy (eV)	Al	Ti
$L1_2$-Al_3Ti at 0 GPa			
1	−10.70	*s* 85.92%; *p* 8.27%	*s* 5.51%; *p* 0.28%; *d* 0.02%
2	−3.06	*s* 9.90%; *p* 61.10%	*s* 1.36%; *p* 6.95%; *d* 20.67%
3	−2.16	*s* 4.06%; *p* 56.85%	*s* 0.56%; *p* 2.76%; *d* 35.77%
4	0.14	*s* 4.47%; *p* 26.55%	*s* 4.75%; *p* 4.12%; *d* 60.12%
$L1_2$-Al_3Ti at 40 GPa			
1	−12.14	*s* 91.79%; *p* 7.91%	*s* 0.22%; *p* 0.05%; *d* 0.02%
2	−3.66	*s* 9.16%; *p* 61.20%	*s* 0.64%; *p* 6.17%; *d* 22.83%
3	−2.31	*s* 3.15%; *p* 57.02%	*s* 0.25%; *p* 1.32%; *d* 38.27%
4	0.09	*s* 3.87%; *p* 27.68%	*s* 5.05%; *p* 4.56%; *d* 58.85%

Note: for $D0_{22}$-Al_3Ti, Al1 refers to Al atoms in the same (001) plane with Ti atoms, and Al2 refers to Al atoms in the (001) plane occupied by themselves.

4. Summary

The structure, formation energy, elastic constants, Debye temperature and electronic structure of $D0_{22}$- and $L1_2$-Al_3Ti have been investigated with respect to external pressure by using first-principles calculations, and the pressure range is 0–40 GPa. The results show that (1) the $L1_2$-Al_3Ti will be stable when the pressure is around 20–30 GPa, the volume drop is about 1% along with the phase transition; (2) the elastic moduli, ductility, anisotropy index and Debye temperature of both phases increase with the pressure going up, and $L1_2$-Al_3Ti has better ductility, smaller anisotropy and lower Debye temperature than $D0_{22}$-Al_3Ti at the pressure range of 0–40 GPa; (3) the Ti-3d delocalization of Ll_2-$A1_3Ti$ under high pressure will strengthen the hybridization between Ti-3d and Al(s,p), which leads to stronger atomic bonding, and subsequently makes the $L1_2$-Al_3Ti more stable under high pressure.

Acknowledgements

The authors acknowledge the financial support for the research from the material processing key subject of Xi'an Shiyou University (YS32030203) and Technology Creative Foundation of Xi'an Shiyou University (Z08038).

References

[1] Y.V. Milman, D.B. Miracle, S.I. Chugunova, I.V. Voskoboinik, N.P. Korzhova, T.N. Legkaya, Y.N. Podrezov, Intermetallics 9 (2001) 839.
[2] S.S. Nayak, S.K. Pabi, B.S. Murty, J. Alloy. Comp. 492 (2010) 128.
[3] C. Amador, J.J. Hoyt, B.C. Chakoumakos, D. de Fontaine, Phys. Rev. Lett. 74 (1995) 4955.
[4] M. Jahnátek, M. Krajčí, J. Hafner, Phys. Rev. B 76 (2007) 14110.
[5] M. Yamaguchi, Y. Umakoshi, T. Yamane, Philos. Mag. 55 (1987) 301.
[6] D.G. Morris, R. Lerf, M. Leboeuf, Acta Mater. 43 (1995) 2825.
[7] T. Takahashi, K. Tominaga, Y. Tsuchida, S. Motizuki, F. Kawai, T. Hasegawa, Mater. Sci. Eng. A. – Struct. 329–33 (1) (2002) 474.
[8] S.Y. Liu, R.Z. Hu, D.L. Zhao, C.Y. Wang, P. Luo, Z.J. Pu, J. Mater. Sci. Technol. 11 (1995) 369.
[9] S.S. Nayak, B.S. Murty, Mater. Sci. Eng. A. – Struct. 36 (7) (2004) 218.
[10] N. Durlu, O.T. Inal, J. Mater. Sci. 27 (1992) 3225.
[11] J. Douin, K. Sharvan Kumar, P. Veyssière, Mater. Sci. Eng. A. – Struct. 192–19 (3) (1995) 92.
[12] S. Wang, P. Guo, L. Yang, F. Zhao, Y. Wang, Mater. Des. 30 (2009) 704.
[13] H. Mabuchi, H. Morimoto, A. Kakitsuji, H. Tsuda, T. Matsui, K. Morii, Scripta Mater. 44 (2001) 2503.
[14] G. Ghosh, A. van de Walle, M. Asta, J. Phase Equilib. Diff. 28 (2007) 9.
[15] M.V. Karpets, Y.V. Milman, O.M. Barabash, N.P. Korzhova, O.N. Senkov, D.B. Miracle, T.N. Legkaya, I.V. Voskoboynik, Intermetallics 11 (2003) 241.
[16] S. Wang, C. Li, W. Yong, X. Hou, H. Geng, F. Xu, Mater. Charact. 59 (2008) 440.
[17] Z. Fang, I.V. Solovyev, H. Sawada, K. Terakura, Phys. Rev. B 59 (1999) 762.
[18] L. Stixrude, C. Lithgow-Bertelloni, B. Kiefer, P. Fumagalli, Phys. Rev. B 75 (2007) 024108.
[19] A. Mujica, R.J. Needs, Phys. Rev. B 55 (1997) 9659.
[20] A.V. Ponomareva, A.V. Ruban, O.Y. Vekilova, S.I. Simak, I.A. Abrikosov, Phys. Rev. B 84 (2011) 094422.
[21] S.J. Clark, M.D. Segall, C.J. Pickard, P.J. Hasnip, M.J. Probert, K. Refson, M.C. Payne, Z. Kristallogr. 220 (2005) 567.
[22] M.D. Segall, P.J.D. Lindan, M.J. Probert, C.J. Pickard, P.J. Hasnip, S.J. Clark, M.C. Payne, J. Phys. – Condens. Mater. 1 (4) (2002) 2717.
[23] P. Hohenberg, W. Kohn, Phys. Rev. B 136 (1964) 864.
[24] M. Levy, Proc. Natl. Acad. Sci. USA 76 (1979) 6062.
[25] D. Vanderbilt, Phys. Rev. B 41 (1990) 7892.
[26] J.P. Perdew, K. Burke, M. Ernzerhof, Phys. Rev. Lett. 77 (1996) 3865.
[27] J.P. Perdew, Y. Wang, Phys. Rev. B 45 (1992) 13244.
[28] J.P. Perdew, J.A. Chevary, S.H. Vosko, K.A. Jackson, M.R. Pederson, D.J. Singh, C. Fiolhais, Phys. Rev. B 46 (1992) 6671.
[29] J.P. Perdew, A. Zunger, Phys. Rev. B 23 (1981) 5048.
[30] D.M. Ceperley, B.J. Alder, Phys. Rev. Lett. 45 (1980) 566.
[31] G. Ghosh, M. Asta, Acta Mater. 53 (2005) 3225.
[32] M. Jahnátek, M. Krajčí, J. Hafner, Phys. Rev. B 76 (2007) 014110.
[33] G. Zhu, Y. Dai, D. Shu, J. Wang, B. Sun, J. Phys. – Condens. Mater. 2 (1) (2009) 415503.
[34] B.G. Pfrommer, M. Côté, S.G. Louie, M.L. Cohen, J. Comput. Phys. 131 (1997) 233.
[35] C. Colinet, A. Pasturel, Intermetallics 10 (2002) 751.
[36] M. Asta, D. de Fontaine, M. van Schilfgaarde, M. Sluiter, M. Methfessel, Phys. Rev. B 46 (1992) 5055–5072.
[37] S. Kurth, J.P. Perdew, P. Blaha, Int. J. Quantum Chem. 75 (1999) 889.
[38] F. Gao, E.J. Bylaska, W.J. Weber, Phys. Rev. B 70 (2004) 245208.
[39] D.J. Siegel, L.G. Hector, J.B. Adams, Surf. Sci. 498 (2002) 321.
[40] R. Ahmed, Fazal-e-Aleem, S.J. Hashemifar, H. Akbarzadeh, Physica B 403 (2008) 1876.
[41] A.J. Du, S.C. Smith, X.D. Yao, G.Q. Lu, J. Phys. Chem. B 109 (2005) 18037.
[42] P. Tang, B. Tang, Solid State Commun. 152 (2012) 1939.
[43] G. Ghosh, S. Vaynman, M. Asta, M.E. Fine, Intermetallics 15 (2007) 44.
[44] M. Jahnátek, M. Krajčí, J. Hafner, Phys. Rev. B 71 (2005) 024101.
[45] M. Nakamura, K. Kimura, J. Mater. Sci. 26 (1991) 2208.
[46] J. Wang, S. Shang, Y. Wang, Z. Mei, Y. Liang, Y. Du, Z. Liu, Calphad 35 (2011) 562.
[47] P. Norby, N. Christensen, Acta Chemica Scandinavica A 40 (1986) 157.
[48] R.E. Watson, M. Weinert, Phys. Rev. B 58 (1998) 5981.
[49] R. Boulechfar, S. Ghemid, H. Meradji, B. Bouhafs, Phys. B 405 (2010) 4045.
[50] M. Nassik, F.Z. Chrifi-Alaoui, K. Mahdouk, J.C. Gachon, J. Alloy Comp. 350 (2003) 151.
[51] T. Hong, T.J. Watson-Yang, A.J. Freeman, T. Oguchi, J. Xu, Phys. Rev. B 41 (1990) 12462.
[52] G. Ghosh, Acta Mater. 55 (2007) 3347.
[53] S.F. Sousa, P.A. Fernandes, M.J. Ramos, J. Phys. Chem. A 111 (2007) 10439.
[54] A. Hao, T. Zhou, Y. Zhu, X. Zhang, R. Liu, Mater. Chem. Phys. 129 (2011) 99.
[55] Y. Ma, A.R. Oganov, Z. Li, Y. Xie, J. Kotakoski, Phys. Rev. Lett. 102 (2009) 065501.
[56] Y. Duan, Y. Sun, M. Peng, Z. Guo, Solid State Sci. 13 (2011) 455.
[57] J. Haines, J.M. Léger, G. Bocquillon, Annu. Rev. Mater. Res. 31 (2001) 1.
[58] J.P. Watt, L. Peselnick, J. Appl. Phys. 51 (1980) 1525.
[59] A.I. Lurie, Theory of Elasticity, Springer, Berlin, 2005.
[60] S.F. Pugh, Philos. Mag. 45 (1954) 823.
[61] S.I. Ranganathan, M. Ostoja-Starzewski, Phys. Rev. Lett. 101 (2008) 055504.
[62] G. Grimvall, Thermophysical Properties of Materials, Elsevier, Amsterdam, 1999.
[63] Z. Witczak, V.A. Goncharova, P. Witczak, J. Alloy Comp. 337 (2002) 58.
[64] M. Jahnátek, M. Krajčí, J. Hafner, Philos. Mag. 87 (2007) 1769.